# Active Disturbance Rejection Control of Electro-mechanical Braking System Using Improved Whale Optimization Algorithm

Zhen Lei, Hongming Lyu*, Lanxiang Zhang, Fusheng Ding

*Abstract*—**To improve the response speed and disturbance rejection capability of the electro-mechanical braking (EMB) system, this paper proposes a control strategy based on the active disturbance rejection control (ADRC) algorithm. First, a three-stage closed-loop control system is designed, which includes brake clearance elimination, clamping force tracking, and brake clearance regeneration. For the critical stage of clamping force tracking, an ADRC is introduced to improve the adaptability and stability of the system to dynamic changes. Next, to address the difficulty of parameter tuning for the ADRC, an improved whale optimization algorithm (WOA) is developed with enhancements to its adaptive inertia weights and nonlinear convergence factors. Finally, comprehensive simulations of all three operational stages of the EMB system are conducted in the Matlab/Simulink environment to validate the effectiveness of the proposed strategy. The simulation results show that the improved WOA significantly enhances both optimization efficiency and control accuracy, leading to notable performance improvements in the EMB system.**

*Index Terms*—**Active disturbance rejection control, Electro-mechanical braking system, Improved whale optimization algorithm, Three-stage closed-loop control.**

## I. Introduction

In recent years, the rapid growth in global automobile ownership has significantly enhanced daily convenience while simultaneously giving rise to pressing social challenges, including energy shortages, environmental pollution, and traffic congestion [1]. Electric vehicles (EVs) have emerged as a promising solution, garnering considerable attention due to their zero-emission characteristics, simplified structural design, and regenerative braking capabilities, which improve overall energy efficiency and extend driving range [2]. To align with the evolving trends of automotive electrification, intelligence, and connectivity, modern braking systems must incorporate advanced features such as brake-by-wire technology [3]. Among these, electro-mechanical braking (EMB) systems offer distinct advantages over traditional hydraulic systems, including a compact structure, rapid response times, and seamless integration with vehicle dynamics control (VDC) systems [4]. These attributes are increasingly critical for advanced intelligent driving applications, positioning EMB as a key focus area for automotive manufacturers [5].

Recent advancements in EMB systems have primarily targeted improvements in clamping force estimation and control strategies. Park et al. utilized an angle sensor to measure motor rotation and estimated clamping force based on the functional relationship between the two [6]. Fu measured the displacement of the ball screw and then estimated the clamping force [7]. Ki adopted a pressure-speed loop and a position-speed loop to switch the control according to the braking state [8]. Chin proposed an active brake judder attenuation strategy by using EMB, and designed two attenuation algorithms to compensate the clamping force [9]. Chris applied model predictive control theory to improve the structure of a three-loop PID controller [10]. Li introduced a novel clamping force model based on linear transformations of polynomial functions and proposed a unified architecture to ensure smooth transitions between gap closing and clamping force tracking [11]. Wei applied direct torque control technology to the permanent magnet synchronous motor (PMSM) in EMB systems, achieving superior clamping force control in EMB actuators [12].

Active disturbance rejection control (ADRC), proposed by Han, has gained widespread adoption as a robust nonlinear control method due to its model-independent nature and strong resilience to uncertainties [13]. Liu introduced a nonlinear multi-input and multi-output (MIMO) decoupling algorithm for PMSMs based on ADRC to address the nonlinearities, strong coupling, and uncertainties associated with these motors [14]. Liu applied active disturbance rejection to control the d$q$-axis current of a PMSM [15]. Wang combined ADRC with a quasi-resonant controller for speed control of a PMSM, which operates in parallel with an extended state observer to achieve smooth speed control [16]. Zhang proposed a sensorless vector active ADRC control method for PMSM using a Luenberger observer, which reduced the steady-state error in speed control and demonstrated strong disturbance rejection capability [17].

While ADRC effectively addresses the trade-off between motor response speed and overshoot inherent in traditional PID control, its parameter tuning remains a significant challenge, hindering broader application [18]. Sun developed an optimal PMSM control strategy using state feedback control optimized by a gray wolf optimization algorithm, achieving faster response and reduced overshoot compared to

Manuscript received Dec 17, 2024; revised Jul 12, 2025.

This work was supported in part by the National Natural Science Foundation of China under Grant 51875494.

Z. Lei is a postgraduate student of School of Automotive Engineering, Yancheng Institute of Technology, Yancheng, 224051, China (e-mail: lei_713@163.com).

H. Lyu* is a professor of School of Automotive Engineering, Yancheng Institute of Technology, Yancheng, 224051 China (corresponding author to provide e-mail: hongming_lv@ycit.edu.cn).

L. Zhang is a postgraduate student of School of Automotive Engineering, Yancheng Institute of Technology, Yancheng, 224051 China (e-mail: 1851900300@qq.com).

F. Ding is a lecturer of School of Automotive Engineering, Yancheng Institute of Technology, Yancheng, 224051 China (e-mail: dfs_ycit@163.com).

conventional PI controllers [19]. Ekinci introduced the Henry gas solubility optimization algorithm based on opposition learning, which was used to determine the optimal parameters for a PID controller to control DC motors, demonstrating excellent control performance and robustness under uncertain system and load disturbance conditions [20]. Hu applied particle swarm optimization to enhance damping characteristics in power system speed control, significantly improving system performance [21]. Wang an improved firefly algorithm for PID controller optimization in brushless DC (BLDC) motors, achieving enhanced robustness and steady-state response [22].

The whale optimization algorithm (WOA), introduced by Mirjalili in 2016, has gained recognition for its simplicity, minimal parameter requirements, and strong ability to escape local optima [23]. However, its limitations, including slow convergence and susceptibility to local optima, necessitate further improvements. Common enhancement strategies include directional learning-based population initialization, adaptive inertial weights, chaotic compilation strategies, and normal variation algorithms. Yousri demonstrated the effectiveness of an improved chaotic WOA in PMSM parameter estimation under both noisy and noise-free conditions, outperforming the standard WOA in efficiency, reliability, and accuracy [24]. Aguilar applied WOA to optimize PI controller parameters, improving linear tuning performance [25]. Choi developed a sliding mode controller using WOA for switching gain adjustment, effectively reducing tracking errors [26].

Despite these advancements, current research on EMB systems remains predominantly focused on clamping force estimation, with limited progress in precise control strategies. Traditional PID control struggles to achieve rapid stabilization following disturbances. To address these limitations, this study proposes a three-stage closed-loop control system for EMB, incorporating a pressure loop control strategy based on the ADRC algorithm. Furthermore, the ADRC parameters are optimized using an improved WOA, aiming to enhance system response speed and control precision.

## II. Modeling

### A. Structure and Working Principle of EMB

Unlike traditional hydraulic braking, EMB represents a mechatronic solution that replaces conventional hydraulic power structures with a torque motor for vehicle braking. The EMB system is primarily composed of several key components: an on-board power supply, a brake pedal unit, a central control unit, an on-board computer network, a control unit, and an actuator. The actuator itself integrates critical elements such as a drive motor, planetary gear, ball screw, and mechanical brake components [27]. A detailed schematic of the EMB actuator's structure (disc type) is illustrated in Fig. 1.

### B. Electromagnetic Properties

A PMSM is selected as the driving motor of the EMB, which is a nonlinear system. After coordinate transformation,

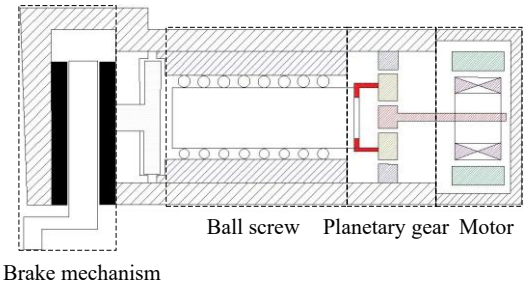


Fig. 1. Structure of the EMB actuator

the voltage equation is as follows [28]:

$$\begin{cases} u_A = R_s i_A + p\psi_A \\ u_B = R_s i_B + p\psi_B \\ u_C = R_s i_C + p\psi_C \end{cases} \tag{1}$$

The flux linkage equation is:

$$\begin{cases} \psi_A = L_{AA} i_A + M_{AB} i_B + M_{AC} i_C + \psi_f \cos\theta \\ \psi_B = M_{BA} i_A + L_{BB} i_B + M_{BC} i_C + \psi_f \cos(\theta - \frac{2\pi}{3}) \\ \psi_C = M_{CA} i_A + M_{CB} i_B + L_{CC} i_C + \psi_f \cos(\theta - \frac{4\pi}{3}) \end{cases} \tag{2}$$

where $u_A$, $u_B$, $u_C$ are the voltage of each phase of the motor, $i_A$, $i_B$, $i_C$ are the current of each phase of the motor, $R_s$ are the resistance of the motor, $L_{AA}$, $L_{BB}$, $L_{CC}$ are the self-inductance of each phase winding of the stator, $M_{AB}$, $M_{BA}$, $M_{AC}$, $M_{CA}$, $M_{BC}$, $M_{CB}$ are the mutual inductance between each phase winding of the stator, and $\psi_A$, $\psi_B$, $\psi_C$ are the three-phase stator flux of the motor. $\psi_f$ is the permanent magnet flux of motor rotor.

### C. Frictional Behavior

The Stribeck model is adopted to describe the friction damping behavior of the drive motor. Its mathematical expression is as follows [29]:

$$T_f = \begin{cases} T_f(\omega) & \omega \neq 0 \\ T_e & \omega=0,\ |T_e| < T_s \\ T_s \operatorname{sgn}(T_e) & \omega=0,\ |T_e| \geq T_s \end{cases} \tag{3}$$

where $T_f(\omega)$ is the function describing the Stribeck phenomenon, $T_s$ is the maximum static friction torque, $T_e$ is the system static friction torque, and $\omega$ is the motor speed.

The Gauss model is used as the function to describe the Stribeck effect. The mathematical expression is:

$$T_f(\omega) = \left(T_c + (T_s - T_c) e^{-(\omega/v_s)^{\sigma_1}}\right) \operatorname{sgn}(\omega) + \sigma\omega \tag{4}$$

### D. Load Torque

The torque output of the drive motor, through the transmission mechanism, is finally transformed into the clamping force on both sides of the brake disc. At the same time, the generated clamping force will also react on the drive motor to form the load torque. The mathematical expression is:

$$F_n = \begin{cases} A\Delta s^3 + B\Delta s^2 - C\Delta s + D & \Delta s > 0.18\Delta s \\ E\Delta s & 0 < \Delta s \leq 0.18 \\ 0 & \Delta s < 0 \end{cases} \tag{5}$$

Then, the load torque of the clamping force acting on the motor is:

$$T_l = \frac{F_n \times L}{2 \times \pi \times \eta_s \times \eta_p \times i_p} \tag{6}$$

where $F_n$ is the clamping force, $\Delta s$ is the difference between the screw nut displacement $s$ and the brake clearance $s_w$, $T_l$ is the load torque, $L$ is the lead of the ball screw, $\eta_s$ is the transmission efficiency of the ball screw, $\eta_p$ is the transmission efficiency of the planetary gear, and $i_p$ is the reduction ratio of the planetary gear.

### *E. Transmission Mechanism*

The EMB transmission mechanism consists of a planetary gear and a ball screw. Its transmission ratio is:

$$s = \frac{\theta \times L}{2 \times \pi \times i_p} \tag{7}$$

where $\theta$ is the motor angle.

## III. Control Strategy

The EMB system completes the whole braking process in three stages: brake clearance elimination, clamping force tracking, and brake clearance regeneration [30]. Consequently, a closed-loop control is implemented for all three stages, with a particular emphasis on the second stage, where an ADRC strategy is designed to enhance the accuracy of clamping force tracking.

### *A. Brake Clearance Elimination*

Control of the drive motor is critical to the EMB system, as it necessitates a rapid response to system inputs. During the brake clearance elimination stage, the motor primarily works to overcome its own frictional resistance. To efficiently eliminate the brake clearance, the target speed is set to the motor's maximum speed, utilizing a speed-current dual-loop control approach.

### *B. Clamping Force Tracking*

After the brake clearance is eliminated, the brake pads engage the brake disc to generate clamping force. The effectiveness of control at this stage not only influences the stopping distance and stability of the vehicle, but also affects passenger comfort. To enhance the accuracy of clamping force tracking and minimize system overshoot, a three closed-loop clamping force-speed-current ADRC system is designed.

The ADRC method consolidates all uncertain factors affecting the controlled object into unknown disturbances. It estimates and compensates for these disturbances using the input and output data from the controlled object [31]. This control system mainly consists of a tracking differentiator (TD), an extended state observer (ESO), and nonlinear state error feedback (NLSEF). The EMB system is treated as a second-order nonlinear system, and an active disturbance rejection controller is developed.

The equation of state for the second-order system is:

$$\begin{cases} \dot{x}_1 = x_2 \\ \dot{x}_2 = f(x_1, x_2, w(t)) + b \cdot u(t) \\ y = x_1 \end{cases} \tag{8}$$

where $u(t)$, $y$ are input and output, are system state variables, $f$ is the total disturbance synthesized inside and outside the system, and $b$ is the gain.

The TD allows the input signal to transition smoothly from the initial value to the target value, with the duration of the transition process adjustable. Both the transition process and the differentiator are implemented in a single module. Its discrete algorithm is:

$$\begin{cases} f(h) = \text{fhan}(x_1(k) - v(k), x_2(k), r, h_0) \\ x_1(k+1) = x_1(k) + h x_2 k \\ x_2(k+1) = x_2(k) + h f h \end{cases} \tag{9}$$

where $x_1$ is the tracking signal of the input signal, $x_2$ is the differential signal of the input signal, $h$ is the sampling period, $v(k)$ is the target signal of the input, and fhan is a fastest synthetic function, defied as follows:

$$\begin{cases} d = r h_0^2 \\ a_0 = h_0 x_2 \\ a_1 = \sqrt{d(d + 8|y|)} \\ a_2 = a_0 + \text{sgn}(y)(a_1 - d)/2 \\ y = x_1 + a_0 \\ s_y = \dfrac{(\text{sgn}(y+d) - \text{sgn}(y-d))}{2} \end{cases} \tag{10}$$

$$\begin{cases} a = (a_0 + y - a_2) s_y + a_2 \\ s_a = \dfrac{(\text{sgn}(a+d) - \text{sgn}(a-d))}{2} \\ \text{fhan} = -r(a/d - \text{sgn}(a)) s_a - r\,\text{sgn}(a) \end{cases} \tag{11}$$

where $r$ is the speed factor and $h_0$ is the filter factor.

The ESO reformulates the total disturbance of the system as a new state variable, which is then estimated and compensated for using the system's inputs, outputs, and applied control inputs. Its mathematical expression is:

$$\begin{cases} e(k) = z_1(k) - y(k) \\ z_1(k+1) = T(z_2(k) - \beta_{01} e(k)) + z_1(k) \\ z_2(k+1) = T\begin{pmatrix} z_3(k) + b_0 u + f_0(z_1, z_2) \\ + \beta_{02} \cdot \text{fal}(e, 0.5, \delta) \end{pmatrix} + z_2(k) \\ z_3(k+1) = T(-\beta_{03} \cdot \text{fal}(e, 0.25, \delta)) + z_3(k) \end{cases} \tag{12}$$

$$\text{fal}(e, \alpha, \delta) = \begin{cases} \dfrac{e}{\delta^{1-\alpha}} \\ |e|^{\alpha}\,\text{sgn}(e) \end{cases} \tag{13}$$

where $z_1(t)$ and $z_2(t)$ are the estimated values of the system state variables $x_1(t)$ and $x_2(t)$, respectively, and $z_3(t)$ represents the observed values of the expanded disturbed state variables. The parameters $\beta_{01}$, $\beta_{02}$, $\beta_{03}$ and $\delta$ are the control parameters, while $\alpha$ is the control parameter of the function fal.

The NLSEF control is particularly effective for systems with unknown exact models. The error between the tracking signal $x_1$ and the differential signal $x_2$ generated by the tracking differentiator, along with the corresponding state variable estimates $z_1$ and $z_2$ produced by the extended state observer, serves as input to the nonlinear feedback controller. This configuration results in a closed-loop control system,

and the algorithm is outlined below:

$$\begin{cases} e_1 = x_1 - z_1 \\ e_2 = x_2 - z_2 \\ u_0 = k\left(e_1, e_2, p\right) \end{cases} \tag{14}$$

$$\begin{aligned} u_0 &= \beta_1 \operatorname{fal}\left(e_1, a_1, \delta\right) + \beta_2 \operatorname{fal}\left(e_2, a_2, \delta\right) \\ 0 &< a_1 < 1 < a_2 \end{aligned} \tag{15}$$

where $u_0$ is the error feedback control quantity, $k$ is the error feedback rate, $\beta_1$ and $\beta_2$ are the control parameters.

The output of the ADRC in the clamping force loop represents the target value for the q-axis current of the PMSM. Therefore, the expression for the clamping force control is as follows:

$$i_q = \frac{u_0 - z_3(t)}{b_0} = \frac{\beta_1 \operatorname{fal}\left(e_1, a_1, \delta\right) + \beta_2 \operatorname{fal}\left(e_2, a_2, \delta\right)}{b_0} \tag{16}$$

### C. Brake Clearance Regeneration

After the clamping force tracking stage ends, the target clamping force becomes zero. Due to the internal friction within the system and the lack of a clearance self-adjustment mechanism in the EMB system, it is necessary to reverse the motor to separate the brake pad from the brake disc, thereby creating a fixed brake clearance. This stage employs a position-speed-current three closed-loop control system.

## IV. Optimization

The ADRC algorithm exhibits strong robustness. However, its parameter tuning relies heavily on the experience of the designer. To further alleviate the challenges associated with parameter tuning in practical applications, the improved WOA is used to select and optimize the parameters of the ADRC.

### A. WOA Principle

The WOA is a novel heuristic optimization technique that mimics the hunting behavior of humpback whales. In the WOA, each humpback whale's position corresponds to a feasible solution. Humpback whales use a unique hunting strategy known as the bubble net attack foraging method, shown in Fig. 2 [23, 32, 33].

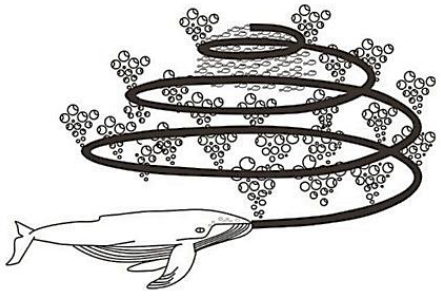

Fig. 2. Bubble-net feeding behavior of humpback whales

When humpback whales detect small fish and shrimp in the ocean, they spiral below and surround their prey with exhaled bubbles. They typically swim in a circular or "9" shape, maximizing their ability to surround the prey and gradually bring it closer until they swallow it all.

During feeding, a group of whales search for prey together. When one whale locates the prey, the others swim over to join in the feeding. In the context of the whale optimization algorithm, each individual whale represents one solution, while a group of whales represents multiple solutions. During the optimization process, these individual whales continuously update their positions until a satisfactory solution is reached.

### B. Whale Optimization Algorithm (WOA)

*Encircling prey*

In the hunting process, whales first observe the location of their prey and then surround it. In the WOA, the optimal solution to the problem is analogous to the position of the lead whale (the prey). Once the best whale position is identified, other whales update their positions by swimming toward that location. Initially, the distance between each individual whale and the optimal whale position (the prey) needs to be calculated.

$$\boldsymbol{D} = |C\boldsymbol{X}^*(t) - \boldsymbol{X}(t)| \tag{17}$$

$$\boldsymbol{X}(t+1) = \boldsymbol{X}^*(t) - A\boldsymbol{D} \tag{18}$$

where $t$ represents the current iteration, $\boldsymbol{X}^*(t)$ denotes the position vector of the best solution obtained so far, $\boldsymbol{X}(t)$ is the position vector at iteration $t$, $\boldsymbol{D}$ is the distance between the current individual whale and the current optimal solution, $A$ and $C$ are two coefficients, which can be calculated as follows:

$$A = 2ar - a \tag{19}$$

$$C = 2r \tag{20}$$

where $r$ is a random number in [0,1], $a$ is a convergence factor that linearly and iterative decreases from 2 to 0 over the course of iterations (in both exploration and exploitation phases).

$$a = 2 - 2t/t_{\max} \tag{21}$$

where $t_{\max}$ is the maximum number of iterations.

*Bubble-net attacking method (exploitation phase)*

The bubble-net method used by humpback whales is unique among all sea creatures. This method is formulated mathematically in two stages: The shrinking encircling mechanism and the spiral updating position.

(a) Shrinking encircling mechanism

This stage is performed utilizing A that decreases in range a and $-a$ to $a$, with the value of a decreasing linearly, as shown in Eq. (19). If $A$ is constrained to the range the range [−1, 1], the current position $X(t)$ of a search agent will be updated to lie between $X(t)$ and the best agent's position $\boldsymbol{X}^*(t)$.

(b) Spiral updating position

In this stage, the distance between the current position of a search agent and the best position is calculated. Subsequently, a spiral is generated using the spiral equation that connects the current position and the best position of the search agents, as follows:

$$\boldsymbol{X}(t+1) = \boldsymbol{X}^*(t) + \boldsymbol{D}_p e^{bl} \cos(2\pi l) \tag{22}$$

where $\boldsymbol{D}_p = |\boldsymbol{X}^*(t) - \boldsymbol{X}(t)|$ is the distance between the current search agent and the best one, $b$ denotes a constant variable used to define the logarithmic spiral' shape, $l$ is a value generated randomly in range [−1, 1].

These whales move around the prey ball or the best positions in a shrinking spiral-shaped path. Accordingly, they can choose to use either shrinking circles or spiral-shaped trajectories based on a 50% probability. This movement and probability are mathematically formulated as follows:

$$\boldsymbol{X}(t+1)=\begin{cases}\boldsymbol{X}^*(t)-A\boldsymbol{D} & p<0.5\\ \boldsymbol{X}^*(t)+\boldsymbol{D}_p e^{bl}\cos(2\pi l) & p\geqslant 0.5\end{cases} \quad (23)$$

where $p$ is the random value in range [0,1].

Search for prey (exploration phase):

Another searching behavior, called exploration, can be utilized in the WOA using the values of $A$. As previously mentioned, the exploitation phase occurs when the value of $A$ is between −1 and 1. Conversely, the exploration phase is executed when $A$ is less than −1 or greater than 1, meaning it falls outside the range [−1, 1]. During this phase, the current search agent will move away from the best search agent and update its position based on a randomly chosen search agent. This phase is mathematically formulated as follows:

$$\boldsymbol{D}=|C\boldsymbol{X}_{\text{rand}}(t)-\boldsymbol{X}(t)| \quad (24)$$

$$\boldsymbol{X}(t+1)=\boldsymbol{X}_{\text{rand}}(t)-A\boldsymbol{D} \quad (25)$$

where $\boldsymbol{X}_{\text{rand}}$ is a random position vector (a random whale) chosen from the current population.

### C. Improved WOA

*Adaptive inertia weight*

In the WOA, the inertia weight w is introduced to enhance the algorithm's convergence to the global optimal solution. A larger inertia weight improves the algorithm's global optimization capability, while a smaller inertia weight enhances its local optimization ability, thus boosting the overall performance of the algorithm. Therefore, this section proposes the use of inertia weight to improve the algorithm. The expression for the inertia weight is as follows:

$$w=\frac{1}{2}\sin\left(\frac{\pi t}{t_{\max}}+\frac{\pi}{2}\right)-\frac{1}{2} \quad (26)$$

Then, the updated formula for the position vector update is as follows:

$$\boldsymbol{X}(t+1)=w\boldsymbol{X}^*(t)-A\boldsymbol{D} \quad p<pi \quad (27)$$

$$\boldsymbol{X}(t+1)=w\boldsymbol{X}^*(t)+\boldsymbol{D}_p e^{bl}\cos(2\pi l) \quad p>pi \quad (28)$$

The inertia weight w d decreases nonlinearly as the number of iterations increases, making the algorithm suitable for global optimization in the early stages and local optimization in the later stages. This approach enhances both the convergence accuracy and the convergence speed.

*Nonlinear convergence factor*

There are two search processes in the WOA: global search and local search. If the performance of these two processes is not well coordinated during population evolution, it can lead to slow convergence or premature convergence of the algorithm. Global search can expand the search area, thereby reducing the probability of the algorithm getting trapped in local optima. Local search involves precise searching in a specific region of the generated population's solution space to accelerate the convergence of the algorithm. The capabilities of global and local search in the WOA are related to the value of A, which changes with the convergence factor a. Therefore, the value of a plays a crucial role in balancing the local and global search capabilities of the algorithm.

The convergence factor $a$ decreases linearly from 2 to 0 as the number of iterations increases. However, the WOA exhibits nonlinear changes during the actual optimization process, so the linear change of the convergence factor cannot accurately reflect the optimization process of the algorithm. To balance the global search and local search capabilities of the algorithm, a new improved scheme for the convergence factor a is proposed:

$$a=\begin{cases}2-e^{\left(\frac{t-1}{t_{\max}-1}\right)^2} & t\leq 0.7t_{\max}\\ 4\dfrac{t_{\max}-t}{t_{\max}-1}-1 & 0.7t_{\max}<t\leq t_{\max}\end{cases} \quad (29)$$

The improved a converges slowly in the early iterations, keeping the parameter $A$ relatively large to enhance global search efficiency. In the later iterations, it converges quickly, allowing the parameter $A$ to remain relatively small, effectively increasing local search efficiency. Therefore, this improved scheme can effectively balance the global and local search performance of the algorithm.

### D. ADRC parameters Tuning by Improved IWOA

Using Matlab/Simulink, a comprehensive control strategy model for EMB is developed (See section 4.1 for details.), alongside the implementation of the program code for the improved WOA. The real-time braking force signal from the EMB system is fed into the improved WOA, enabling the algorithm to generate distinct ADRC parameters during each iteration. The difference between the target clamping force and the real-time clamping force is then evaluated to determine whether the optimal solution has been achieved. If the optimal solution is identified, the iteration process terminates. In this study, three key parameters are optimized: $\beta_{01}$ and $\beta_{02}$ in the ESO, and $\beta_2$ in the NLSEF, need to be optimized in this paper. The detailed flowchart of this process is illustrated in Fig. 3.

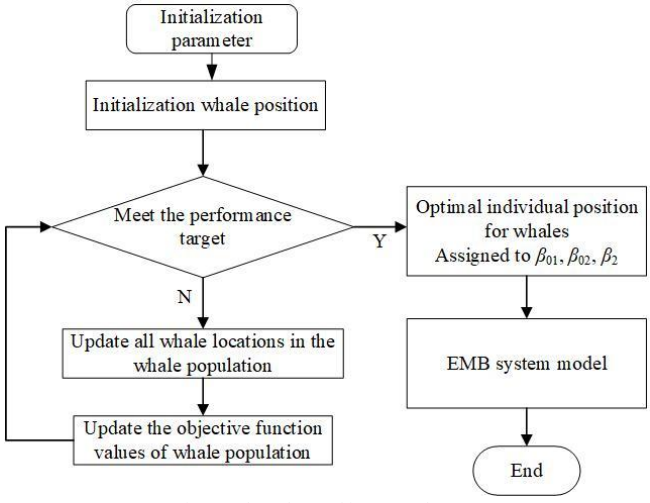


Fig. 3. Flowchart of improved WOA

The algorithm is configured with a population size of 100 and a maximum iteration count of 50. The fitness function is formulated as:

$$J=50\cdot t_r+20\cdot t_s+200\cdot\max\left(0,\frac{F_{\max}-5000}{5000}\right)+10^4\cdot\max(0,t_r-0.1)^2+10^3\cdot\max(0,|e_{ss}|-250)^2 \quad (30)$$

where $t_r$ is braking force rise time，$t_s$ is braking force settling time，$e_{ss}$ is steady-state error.

The optimization results for the self-disturbance parameters are presented in Fig. 4 and Fig. 5. Compared to

the original WOA, the improved algorithm exhibits significantly enhanced convergence speed and fitness, demonstrating its superior performance in parameter optimization.

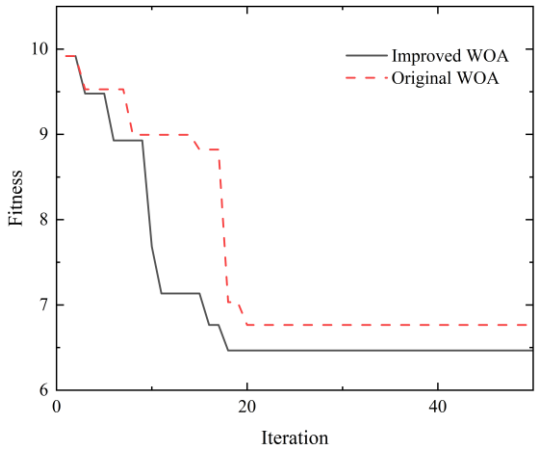


Fig. 4. Fitness evolution of different WOA

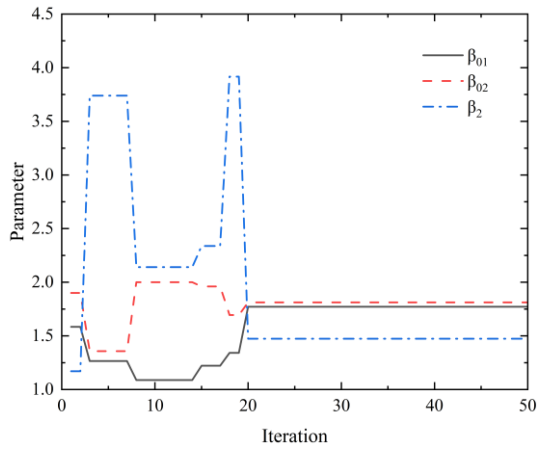


(a) Original WOA

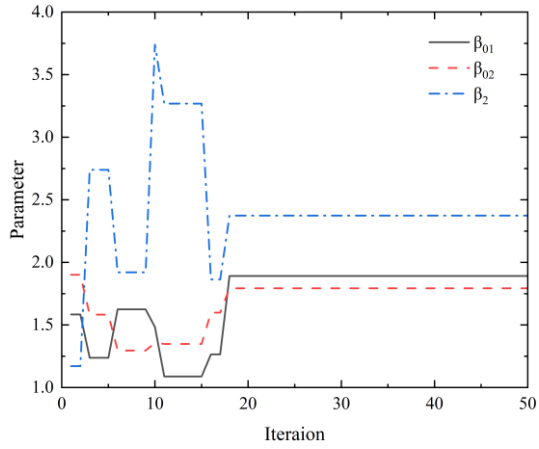


(b) Improved WOA

Fig. 5. Evolution of ADRC parameters using different WOA

The simulation results indicate that the IWOA converges at the 18th iteration, outperforming conventional algorithms by completing optimization two iterations earlier. This corresponds to a 10% reduction in convergence generations and a 4.43% improvement in fitness value of the optimal solution.

## V. Co-simulation Of The EMB

To validate the effectiveness and accuracy of the proposed three-stage closed-loop control strategy and the optimized ADRC algorithm, a comprehensive simulation model was developed in Matlab/Simulink for detailed analysis.

### *A. System Step Response*

By focusing exclusively on the brake clearance elimination and clamping force tracking stages, while disregarding the brake clearance regeneration phase, step signals of 5 kN, 10 kN, 12 kN, and 15 kN were sequentially applied to the EMB system. The corresponding simulation results for clamping force and motor speed responses are shown in Fig. 6.

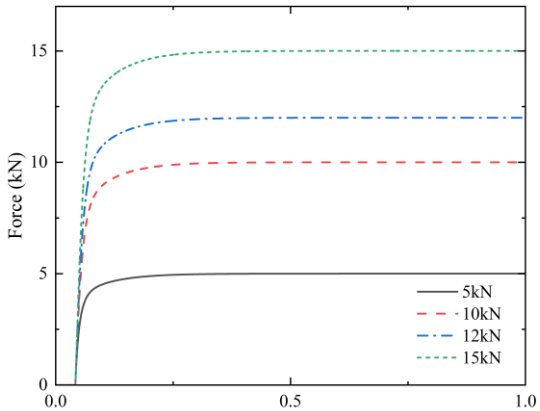


(a) Clamping force

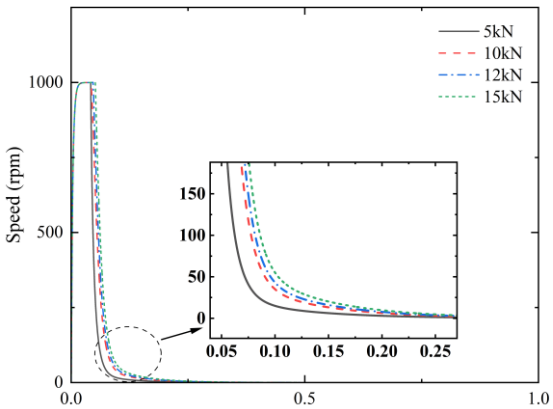


(b) Motor speed

Fig. 6. EMB system responds in real time

The EMB system demonstrated its capability to completely eliminate brake clearance within 0.04 seconds across all four clamping force step inputs, thereby satisfying the specified response requirements for EMB brakes. The system exhibited precise real-time tracking of target clamping forces, maintaining an error margin below 5%. During the brake clearance elimination phase, the motor speed rapidly accelerated to its maximum value, subsequently dropping to zero upon contact between the brake disc and pad, resulting in a locked motor state that exclusively delivered torque output.

Fig. 7 presents comparative simulation results of 5kN step brake force application through four distinct control methods: empirically tuned ADRC, original WOA-tuned ADRC, improved WOA-tuned ADRC, and PID control, along with traditional electro-hydraulic braking system (EHB). The

corresponding controller parameters for these three ADRC tuning approaches and PI controller are detailed in Table 1 and Table 2, respectively.

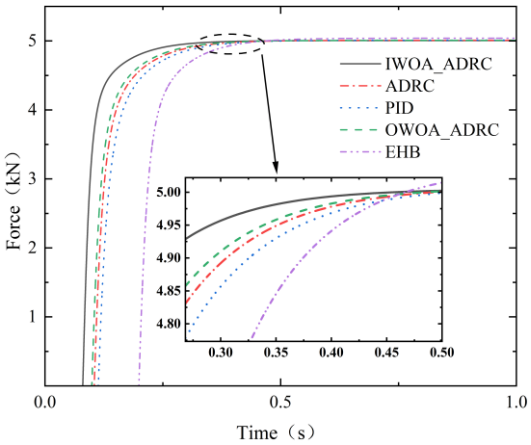


Fig. 7. Comparative analysis of braking force dynamic response

TABLE I
ADRC CONTROLLER PARAMETERS

| Parameters | Empirical-tuned ADRC | Original WOA-tuned ADRC | Improved WOA-tuned ADRC |
|---|---|---|---|
| $\beta_{01}$ | 1.6 | 1.77116 | 1.89155 |
| $\beta_{02}$ | 2.0 | 1.81251 | 1.79272 |
| $\beta_2$ | 1.5 | 1.47371 | 2.37371 |

TABLE II
PI CONTROLLER PARAMETERS

| Parameters | Speed loop | Q-axis current loop | D-axis current loop |
|---|---|---|---|
| P | 1500 | 0.7 | 0.5 |
| I | 10 | 360 | 480 |

Compared to the original WOA-tuned ADRC, empirical ADRC tuning, PID control, and EHB systems, the improved WOA-optimized ADRC demonstrates significant performance enhancements. Specifically, it achieves reductions in brake clearance elimination time by 19.30%, 23.21%, 29.08%, and 59.72%, respectively. Additionally, it improves brake force rise time by 1.69%, 2.58%, 3.94%, and 15.29%, respectively.

### *B. System Three-Stage Response*

A step signal of 5 kN was applied to the EMB system to validate the designed three-stage control strategy, and the simulation results are shown in Fig. 8.

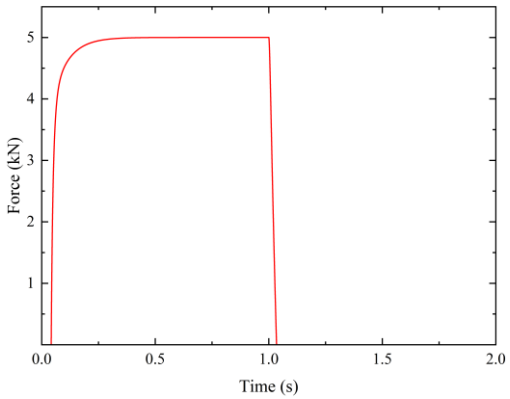


(a) Clamping force

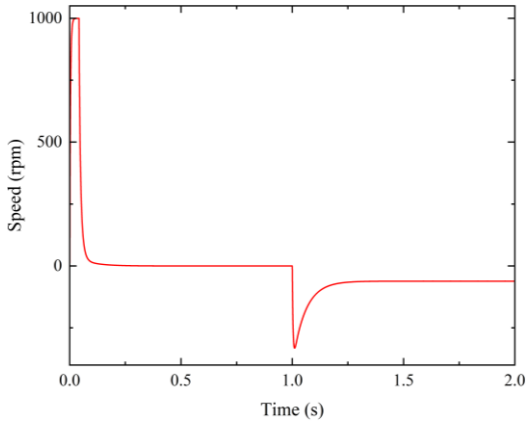


(b) Motor speed

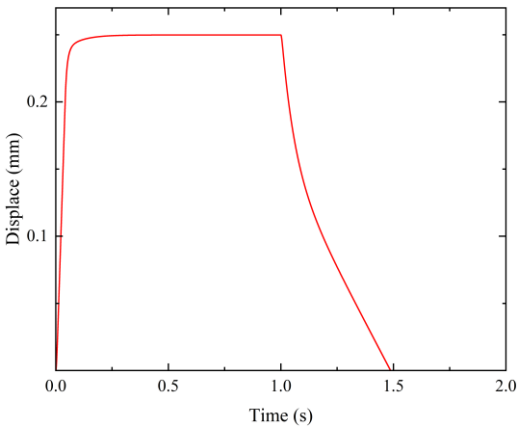


(c) Ball screw displacement

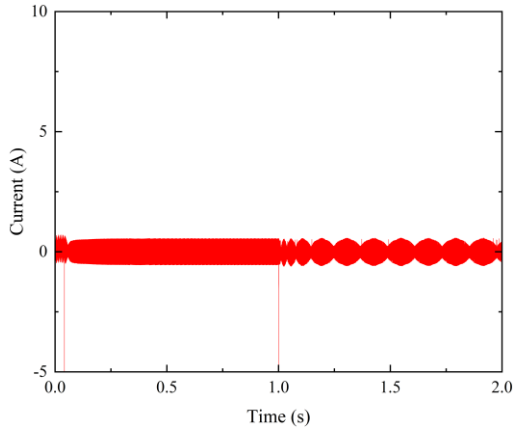


(d) Motor current

Fig. 8. Response of the EMB system upon 5KN input

When the EMB controller receives the braking signal, it quickly increases the motor speed to rapidly eliminate the brake clearance. At 0.02 s, the speed reaches its maximum value of 1000 rpm; at 0.04 s, the brake clearance is completely eliminated and the system enters the force tracking stage where the speed decreases rapidly. At 0.3 s, the braking force reaches the target value and the motor current stabilizes.

At 1 s, a release brake signal is applied to the EMB system, which enters the brake clearance regeneration stage, causing the clamping force to rapidly decrease to zero. Due to the internal friction in the motor, the ball screw cannot return to its initial position, so the motor must reverse a certain angle. After the release brake signal has been applied for 0.5 s, a fixed brake clearance of 0.2 mm is formed to prevent unnecessary friction of the brake pad when braking is not required.

### C. System Disturbance Rejection

The EMB system was evaluated under four distinct control strategies: improved WOA-tuned ADRC, original WOA for ADRC parameter tuning, empirical ADRC parameter tuning, and PID control. A target clamping force of 5 kN was applied, with an intentional load disturbance introduced at 0.5 s. The comparative results of the four strategies are shown in Fig. 9.

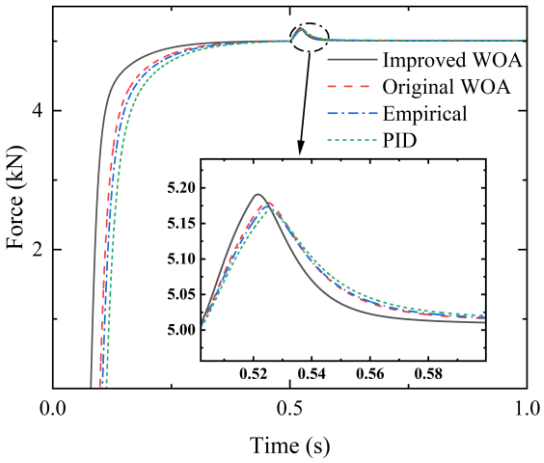


Fig. 9. Disturbance rejection capability of the clamping force

It is found that the improved WOA-tuned ADRC outperforms the other control algorithms, achieving reductions in stabilization recovery time by 3.32%, 3.47%, and 5.03%, respectively, under disturbance conditions.

## VI. Conclusion

In this paper, a three-stage closed-loop control strategy for the EMB is proposed, and an improved WOA is employed to optimize the parameters of ADRC for clamping force tracking. The response characteristics of the EMB system across different braking stages are analyzed through simulation. The results demonstrate that:

The three-stage closed-loop control strategy for the EMB effectively manages the drive motor's rotation during the brake clearance elimination stage, ensuring rapid clearance elimination. During the clamping force tracking stage, it achieves precise and fast tracking of the target force. In the brake clearance regeneration stage, it controls the motor to reverse, establishing a fixed clearance to prevent unnecessary brake friction, thereby enhancing system efficiency and longevity.

The introduction of adaptive inertia weights and a non-linear convergence factor into the WOA significantly enhances its global and local search capabilities while improving convergence efficiency. This optimization allows the algorithm to more effectively balance exploration and exploitation during the parameter tuning process.

By utilizing the improved WOA to tune the ADRC parameters, the EMB system exhibits significant reductions in both brake clearance elimination time and clamping force rise time. Furthermore, the system demonstrates robust disturbance rejection, quickly returning to a stable state after disturbances. These improvements contribute to enhanced braking performance and increased vehicle stability during braking operations.

## References

[1] H. Zhang, B. Xue, L. Chen, L. Wang, K. Huang, Z. Chang, Y. Yu, "The electric vehicles recycling process to carbon neutrality mission in China tends to be negative: Depending on the technology transition," Polish Journal of Environmental Studies, vol. 32, no. 2, pp1941-1948, 2023.

[2] Y. Tang, Q. Zhang, B. Liu, Y. Li, R. Ni, Y. Wang, "What influences residents' intention to participate in the electric vehicle battery recycling evidence from China," Energy, vol. 276, pp127563, 2023.

[3] C. Li, G. Zhuo, C. Tang, L. Xiong, "A review of electro-mechanical brake (EMB) system: structure, control and application," Sustainability, vol.15, no. 5, pp4514, 2023.

[4] Z. Zhang, K. Yang, M. Nie, C. Ma, D. Tan, Z. Huang, "Design and verification of a novel synchronous force-increasing disk electro-mechanical brake actuator for pure electric trucks," International Journal of Automotive Technology, pp1-18, 2025.

[5] S. Schrade, X. Nowak, A. Verhagen, D. Schramm, "Short review of EMB systems related to safety concepts," Actuators, vol. 11, no. 8, pp214, 2022

[6] G. Park, S. Choi, D. Hyun, "Development of clamping force estimation algorithm and clamp-force sensor calibration on electromechanical brake systems," Transactions of the Korean Society of Automotive Engineers, vol. 24, no. 3, pp365-371, 2016.

[7] Y. F. Fu, X. H. Hu, W. R. Wang, Z. Ge, "Simulation and experimental study of a new electromechanical brake with automatic wear adjustment function," International Journal of Automotive Technology, vol. 21, no. 1, pp227-238, 2020.

[8] Y. H. Ki, K. J. Lee, J. S. Cheon, H. S. Ahn, "Design and implementation of a new clamping force estimator in electro-mechanical brake system," International Journal of Automotive Technology, vol. 14, no. 5, pp739-745, 2013.

[9] C. F. Lee, C. Manzie, "Active brake judder attenuation using an electromechanical brake-by-wire system," IEEE/ASME Transactions on Mechatronics, vol. 21, no. 6, pp2964-2976, 2016.

[10] C. Line, C. Manzie, M. C. Good, "Electromechanical brake modeling and control: From PI to MPC," IEEE Transactions on Control Systems Technology, vol. 16, no. 3, pp446-457, 2008.

[11] Y. Li, T. Shim, D. -H. Shin, S. Lee, S. Jin, "Control system design for electromechanical brake system using novel clamping force model and estimator," IEEE Transactions on Vehicular Technology, vol. 70, no. 9, pp8653-8668, 2021.

[12] Z. Wei, J. Xu, D. Halim, "Clamping force control of sensor-less electro-mechanical brake actuator," 2017 IEEE International Conference on Mechatronics and Automation (ICMA), Takamatsu, Japan, 2017, pp. 764-769.

[13] J. Han, "From PID to active disturbance rejection control," IEEE Transactions on Industrial Electronics, vol. 56, no. 3, pp900-906, 2009

[14] Y. Liu, J. Wen, D. Xu, Z. Huang, H. Zhou, "The decoupled vector-control of PMSM based on nonlinear multi-input multi-output decoupling ADRC," Advances in Mechanical Engineering, vol. 12, no. 12, 2020.

[15] X. Liu, G. Zhang, Z. Shi, "Improved current control for PMSM via an active disturbance rejection controller," European Journal of Control, vol. 78, pp101005, 2024.

[16] B. Wang, M. Tian, Y. Yu, Q. Dong, D. Xu, "Enhanced ADRC with quasi-resonant control for PMSM speed regulation considering aperiodic and periodic disturbances," IEEE Transactions on Transportation Electrification, vol. 8, no. 3, pp568-3577, 2022.

[17] P. Zhang, Z. Shi, B. Yu, H. Qi, "Research on a sensorless ADRC vector control method for a permanent magnet synchronous motor based on the Luenberger observer," Processes, vol. 12, no. 5, pp906, 2024.

[18] C. Pu, Z. Wang, S. Wang, "Two-stage active disturbance rejection control for coupled permanent magnet synchronous motors system with mismatched disturbance," International Journal of Control, Automation and Systems, vol. 22, pp1883–1892, 2024.

[19] X. Sun, Z. Jin, Y. Cai, Z. Yang, L. Chen, "Grey wolf optimization algorithm based state feedback control for a bearingless permanent magnet synchronous machine," IEEE Transactions on Power Electronics, vol. 35, no. 12, pp13631-13640, 2020.

[20] S. Ekinci, B. Hekimoğlu, D. Izci, "Opposition based Henry gas solubility optimization as a novel algorithm for PID control of DC motor," Engineering Science and Technology, an International Journal, vol. 24, no. 2, pp331-342, 2021.

[21] Z. Hu, G Yang, "Simulation control model of synchronous motor based on PSO algorithm optimization in power system," Energy Reports, vol. 8, suppl. 4, pp1044-1054, 2022.

[22] Z. Wang, Y. Zhang, P. Yu, N. Cao, H. Dintera, “Speed control of motor based on improved glowworm swarm optimization,” Computers, Materials and Continua, vol. 69, no 1, pp503-519, 2021.
[23] S.Mirjalili, A. ewis, “The whale optimization algorithm,” Advances in Engineering Software, vol. 95, pp51-67, 2016.
[24] D. Yousri, D. Allam, M. B. Eteiba, “Chaotic whale optimizer variants for parameters estimation of the chaotic behavior in permanent magnet synchronous motor,” Applied Soft Computing, vol. 74, pp479-503, 2019.
[25] O. Aguilar-Mejia, R. Sosa-Cortes, C. Enriquez-Ramirez, J. L. Templos-Santos, H. Minor-Popocalt, R. Tapia-Olvera, "Speed Control of PMSM using nature-inspired algorithms," IEEE Latin America Transactions, vol. 16, no. 2, pp. 677-685, 2018
[26] A. Choi, H. Ahn, Y. Chung, K. You, “Sliding mode control for sensorless speed tracking of PMSM with whale optimization algorithm and extended Kalman filter,” Machines, vol. 11, no. 9, pp851, 2023.
[27] K. Yang, L. Chen, Y. Chen, C. Ma, D. Tan, W. Wang, “Structure design and advantage research for bidirectional synchronous force-increasing EMB actuator,” Engineering Research Express, vol. 6, no. 1, pp015051, 2024.
[28] L. Chen, X. Sun, H. Jiang, X. Xu, “High performance control of a permanent magnet synchronous motor for electric vehicle applications,” Journal of Computational and Theoretical Nanoscience, vol. 11, no. 3, pp706-710, 2014.
[29] C. Wang, J. Peng, J. Pan, “A Novel friction compensation method based on Stribeck model with fuzzy filter for PMSM servo systems,” IEEE Transactions on Industrial Electronics, vol. 70, no. 12, pp12124-12133, 2023.
[30] J. Li, W. Mengchun, R. He, and J. Zhang, “A design of electromechanical brake system triple-loop controllers using frequency domain method based on bode plote,” Proceedings 2011 International Conference on Transportation, Mechanical, and Electrical Engineering (TMEE), Changchun, 2011, pp. 795-798.
[31] L. Yu, L. Ding, Q. Xie, F. Yu, "Active disturbance rejection control of position control for electrohydraulic servo system," Engineering Letters, vol. 28, no. 3, pp944-948, 2020.
[32] M. H. Nadimi-Shahraki, H. Zamani, Z. Asghari Varzaneh, S. Mirjalili, “A systematic review of the whale optimization algorithm: theoretical foundation, improvements, and hybridizations,” Archives of Computational Methods in Engineering, vol. 30, no. 7, pp4113-4159, 2023.
[33] S. Mirjalili, “Handbook of whale optimization algorithm variants, hybrids, improvements, and Applications,” Academic Press, 2024.